# Further Analysis of the Composite Wind and Thermodynamic Structure of the 12 September GATE Squall Line

JOHN F. GAMACHE* AND ROBERT A. HOUZE, JR.

*Department of Atmospheric Sciences, University of Washington, Seattle, WA 98195*

(Manuscript received 10 April 1984, in final form 18 March 1985)

ABSTRACT

An objective analysis technique is applied to the time-composite wind and thermodynamic fields of the 12 September GATE tropical squall line. Previous subjective analyses described by Gamache and Houze are confirmed and several new results are obtained.

In the previous analyses, mesoscale upward motion was found in the upper troposphere of the stratiform precipitation region immediately trailing the squall line. Mesoscale downward motion was found in the lower troposphere of the stratiform region. The convective clouds were found to be the source of condensate for more than half of the stratiform precipitation, but mesoscale-updraft condensation was also found to be substantial. In these previous studies, thermodynamic structure was not analyzed, the wind analyses were limited by the number of levels included and vorticity was not analyzed. By employing an objective analysis method in the present study, we have refined and extended the previous work by including more levels, computing vorticity and analyzing the thermodynamic fields.

In the stratiform region, the level of zero vertical motion separating the mesoscale updraft in the upper troposphere from the mesoscale downdraft below is found to be at the 520 mb level (a higher altitude than was indicated by the previous subjective analyses). Maximum convergence in the stratiform region occurred near this level (at 500 mb), but maximum positive vorticity is found to have been at a somewhat lower altitude (650 mb).

The thermodynamic structure of the mesoscale updraft in the stratiform region is indicated by the objective analysis to have been more complex than previously estimated. In its central layer the mesoscale updraft contained a warm anomaly with a humidity that was saturated with respect to ice. Cool anomalies are indicated to have existed near the top of the stratiform cloud deck and (possibly) at the base of the mesoscale updraft.

The structure of the squall system was apparently strongly affected by interaction with the wake of an earlier squall line and with a convective line existing immediately ahead of the squall and intersecting it at nearly right angles. The portion of the squall line feeding on the stabilized wake air associated with these two convective lines was characterized by systematically lower cell tops, as determined by radar, than the remainder of the line. The portion of the stratiform region trailing this part of the line exhibited a distinctly different thermodynamic stratification than was observed to the rear of the deeper-cell section of the squall line. This difference is attributed to the lower altitudes at which condensate and water vapor were determined from this portion of the line are inferred to have advected into the stratiform region.

## 1. Introduction

Studies of tropical squall lines have been one of the primary outcomes of the Global Atmospheric Research Programme's Atlantic Tropical Experiment (GATE) (see reviews by Betts, 1978; Houze and Betts, 1981; Houze and Hobbs, 1982). One of the most comprehensively observed GATE squall lines occurred on 12 September 1974. Aspects of this cloud system have been analyzed by several investigators. Studies of this squall line carried out between 1975 and 1980 are listed in Table 1 of Houze and Betts (1981). More recently it has been the subject of Fitzjarrald and Garstang (1981a,b), Gamache and Houze (1982, 1983), Chen and Zipser (1982) and Johnson and Nicholls (1983), and work is continuing on this case (Zipser, personal communication, 1984). Gamache and Houze (1982, 1983; referred to hereafter as GH1 and GH2) examined the mesoscale air motions and water budget of this squall system. Their studies were accomplished by constructing composite fields of the wind, temperature, specific humidity, radar echo and satellite infrared brightness observed in the vicinity of the squall line over a period of about 9 h. These composite fields were subjectively analyzed at eight pressure levels, and divergence and vertical velocity in the convective and stratiform regions of the squall system were computed kinematically from the subjectively analyzed wind fields. Condensation, evapo-

* Present affiliation: Hurricane Research Division, Atlantic Oceanographic and Meteorological Laboratory, NOAA, Miami, FL 33149.

ration and other quantities involved in the water budget analysis were determined using the computed vertical velocity together with the composite wind, thermodynamic and radar-echo fields.

In this paper, we extend these previous studies by conducting an objective analysis of the composite wind and thermodynamic fields. The method of Barnes (1964, 1973), as applied by Maddox (1980), is used to construct low-pass (synoptic scale) and band-pass (mesoscale) analyses. The purpose of these analyses is to provide confirmation of the previous subjective analyses and add vertical resolution by allowing us to increase the number of levels analyzed from 8 to 19. We also extend our previous research by analyzing thermodynamic fields, calculating vorticity and examining the interaction of the 12 September squall line with an intersecting line of convection and with the wake of an earlier squall line.

## 2. Method of analysis

In GH1 and GH2, the data sources and the method of transferring data into a coordinate system attached to the moving squall line were discussed. In this method, the center of the line is the origin of the moving frame and $\alpha$ labels a coordinate axis normal to the line, while $\beta$ refers to an axis parallel to the line. We refer to a set of data mapped into the $\alpha$–$\beta$ coordinate system as a "composite field." The objective analysis carried out in this study was performed on the composite fields of horizontal wind, temperature and humidity.

The objective analysis procedure we use (see Section 2 of Maddox, 1980, for mathematical details) employs the low-pass method of Barnes (1964). In his technique, each grid point value is determined as a weighted average of all the observations within some specified radius of influence. Each weight is a Gaussian function of the distance between the grid point and the observation, and in our study the radius of influence is infinite, that is, all the observations are used in calculating each grid-point value. Barnes (1973) derived the response of his method to a continuous data field that varies sinusoidally. He also discussed a version of the technique in which a wide Gaussian function is used for the first weighted average (first pass) and a narrower Gaussian weighting is used to analyze the differences between the first-pass analysis and the observations (correction pass). The analysis of the difference field is added to the first-pass field to obtain a corrected analysis. Further correction passes can be made until the desired convergence between the analyzed fields and the observations is obtained. We use this version of Barnes' method in our study.

The advantage of Barnes' objective analysis technique is that the application of the wide Gaussian function during the first pass readily accommodates unevenly spaced data without affecting the wavelength response of the method, while the use of the narrower function in the correction pass produces rapid convergence of the analyzed field to the observed data.

The wavelength response of Barnes' technique is controlled by the choice of weighting functions. Maddox (1980) developed a scheme in which the difference between two low-pass analyses of the same data determines a bandpass analysis. This scheme is described in detail in his article and will only be briefly described here. The low pass analyses were selected so that the bandpass response would be in the mesoscale wavelength range. In our study, we follow the approach of Maddox. We also use the same symbols, referring to the low-pass analysis that retains more of the higher frequencies as F1, while calling the analysis that retains only the lower frequencies F2. The wavelength responses of F1 and F2 are referred to as R1 and R2 and are illustrated in Fig. 1. They represent the fractional reduction of amplitude produced by applying the Barnes low-pass filter to a sinusoidally varying data field. F1 and F2 are designed in our study so that the bandpass response is maximum at a wavelength of 500 km (Fig. 1). This response was chosen after employing the covariance analysis used by Maddox and Vonder Haar (1979). This analysis showed some evidence of important oscillations at 200 km wavelength and then again at 500 km. The shorter wavelength produced an unacceptably noisy response and was probably associated with those observations found near the convective squall lines. The 500 km wavelength bandpass analysis was much less noisy, and it appears to be consistent with the wind field associated with the inflows and outflows associated with the mesoscale vertical motion in the stratiform region (the parameters C1, C2, G1, and G2 are the same as those shown in Maddox, 1980, since his wavelength of maximum response was also 500 km). The winds associated with these inflows and outflows reverse direction and generally increase in intensity outward from their centers over the

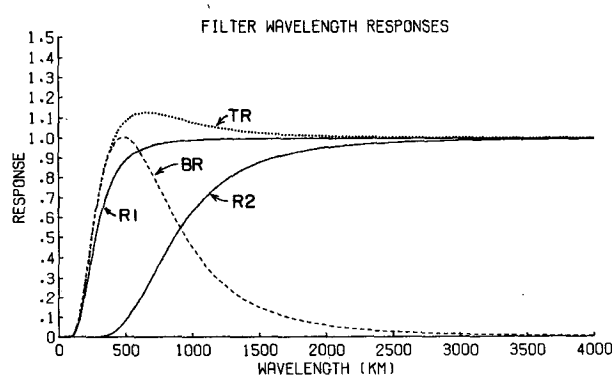


FIG. 1. Response as a function of wavelength of the F1 low-pass (R1), F2 low-pass (R2), mesoscale-bandpass (BR) and total (TR) objective analyses.

distance from the squall line at $\alpha = 0$ to the rear of the stratiform region at $\alpha = 250$ km. Such a reversal represents half of a full oscillation of wind direction. The bandpass field B and its wavelength response BR (Fig. 1) are given by

$$B = \eta(F1-F2), \quad (1)$$

$$BR = \eta(R1-R2) \quad (2)$$

where $\eta$ is a normalization factor assigned the value of the reciprocal of the maximum value of (R1–R2). The total field, called T, is the sum of B and F2, and its response, called TR, equals the sum of BR and R2 (Fig. 1).

The F1, F2, B and T analyses are all presented in the dissertation of Gamache (1983). In this paper, we will concentrate on the bandpass analysis. The composite fields on which the objective analyses are performed have been constructed with respect to the mesoscale squall line. Consequently, the synoptic-scale background pattern is not particularly meaningful. The B analysis, the subtraction of F2 from F1, removes this background while retaining the mesoscale signal. The data domain for the composite fields is an area 1200 km by 1200 km, approximately centered on the origin of the $\alpha$–$\beta$ coordinate system. However, the density of data is sufficient to resolve mesoscale features only within a subregion extending over $\alpha = -200$ to $\alpha = 350$ km and $\beta = -100$ km to $\beta = 300$ km (Fig. 2). This smaller area is the domain of the analyses shown in this paper. The horizontal spacing of grid points is 50 km in both $\alpha$ and $\beta$. Objective analyses were performed at 50 mb intervals from 100 to 900 mb. The 1000 mb and 950 mb levels were also included (for a total of 19 levels) when analyzing thermodynamic fields, while the surface and 960 mb levels were used (for a total of 19 levels) in analyses of the wind field.

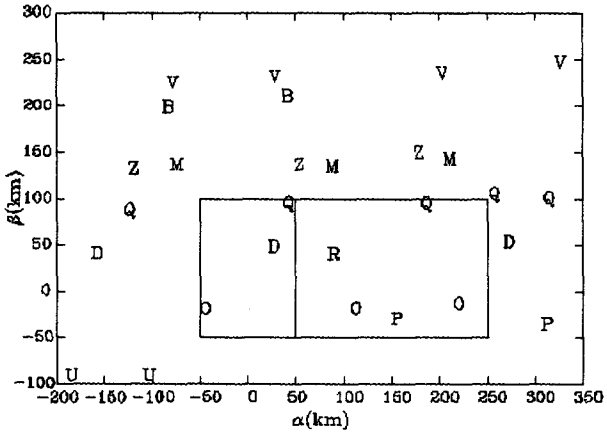


FIG. 2. Locations of rawinsondes within the composite ($\alpha$–$\beta$) coordinate system. Letters indicate name of ship (R—*Researcher*, D—*Dallas*, G—*Gilliss*, O—*Oceanographer*, V—*Vanguard*, Q—*Quadra*, Z—*Vizer*, P—*Poryv*, U—*Zubov*, M—*Meteor* and B—*Bidassoa*).

To analyze the composite wind field, the observed winds are separated into their $\alpha$ and $\beta$ components. Each component is then analyzed in the manner described above. No attempt is made to force vertical continuity; each level is analyzed independently. The vector winds are reconstructed from the analyses of the component fields. The divergence and vorticity are computed at each grid point from the winds at the surrounding four grid points. As in GH2, vertical profiles of divergence and vorticity are computed using a cubic-spline forced to fit the values computed at each pressure level. Although the spline fit is produced in the same manner, it is now forced to fit the values at each of the 19 analyzed levels, giving it more resolution than the profiles shown in GH2. The divergence profiles are then mass-balanced and vertical velocities are computed using the procedures described in GH1.

## 3. Horizontal wind analyses

Analyses of the surface, 650, 500 and 200 mb winds are shown in Figs. 3–6. The area of the squall-line system is indicated on each horizontal map, the smaller rectangle (between $\alpha = -50$ and 50 km) containing the convective region and the larger rectangle (between $\alpha = 50$ and 250 km) containing the stratiform region. These regions are the same as those used in GH1 and GH2.

The bandpass analysis of the surface, 650, 500 and 200 mb winds are shown in Figs. 3, 4, 5a and 6. The total relative wind analysis at 500 mb shown in Fig. 5b is the difference of the total [($T$), not to be confused with the bandpass ($B$) analysis] and the squall-motion vector; it is the objective counterpart to the subjective relative wind analysis at 450 mb given in Fig. 8b of GH1. The bandpass analyses do not have a counterpart in GH1. They separate the large-scale flow features from those associated directly with the moving squall system since large-scale airflow through the squall region is eliminated in the bandpass analysis. Only the perturbations of this flow by the squall system remain. At certain levels this flow may resemble either the observed wind field or the relative wind field; however, the bandpass field does not represent any actual wind field in a ground-relative or system-relative frame of reference.

In the surface analysis (Fig. 3), the primary features are the divergence centered in the stratiform region and the convergence evident in the leading negative $\alpha$ portion of the convective region. In the stratiform region, these features agree well in magnitude and position with those determined by the subjective analysis discussed in GH1, but in the convective region, they agree only fairly well (within 50 km) in position and rather poorly in magnitude. The scale of the bandpass analysis is too broad and the distribution of soundings is too coarse to reproduce the details of convective-scale features.

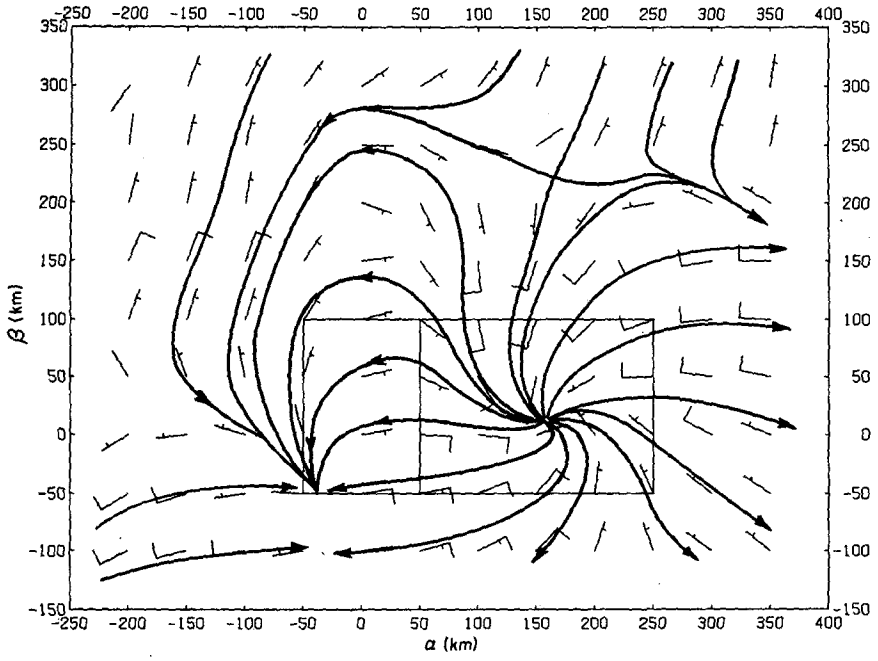


FIG. 3. Mesoscale-bandpass surface wind analysis. Full barb represents 5 m $s^{-1}$.

At 650 mb (Fig. 4), the major feature of the bandpass analysis is the mesoscale convergent cyclonic vortex centered in the stratiform region. At this level, the bandpass wind pattern strongly resembles the *relative* wind pattern (Fig. 7b of GH1). The total observed flow is obtained by adding the squall line motion to the relative flow or by adding the synoptic-scale component to the band-pass flow. Since the squall line motion was roughly equal to the synoptic-scale wind velocity at this level, it is reasonable that the band-pass and relative wind patterns are similar.

The bandpass analysis for 500 mb (Fig. 5a) also shows convergence concentrated in the stratiform region; however, a cyclonic vortex is not evident at this level as it is in Fig. 4. The mesoscale convergence at 500 mb is also seen in the total relative wind

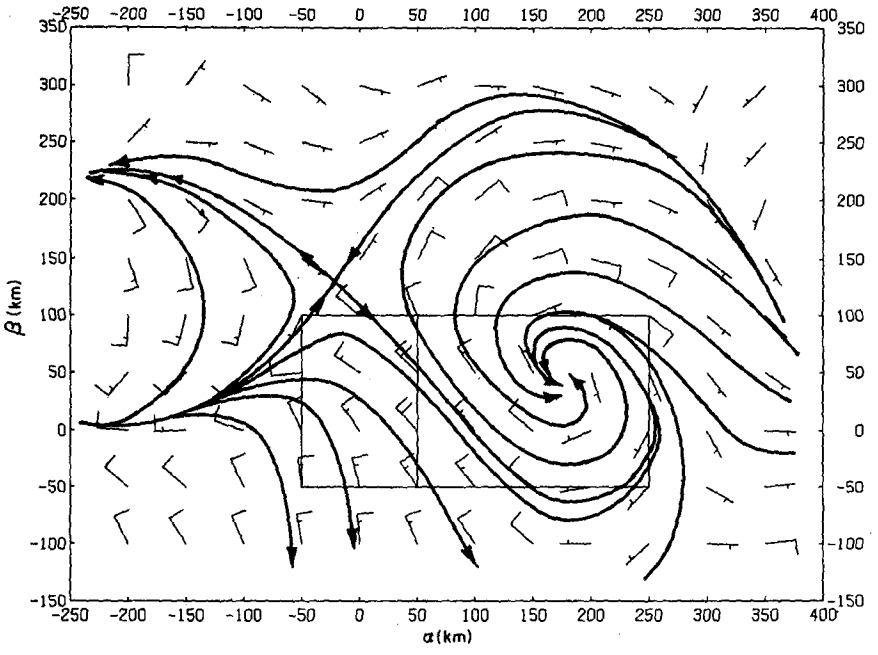


FIG. 4. Mesoscale-bandpass 650 mb wind analysis. Full barb represents 5 m $s^{-1}$.

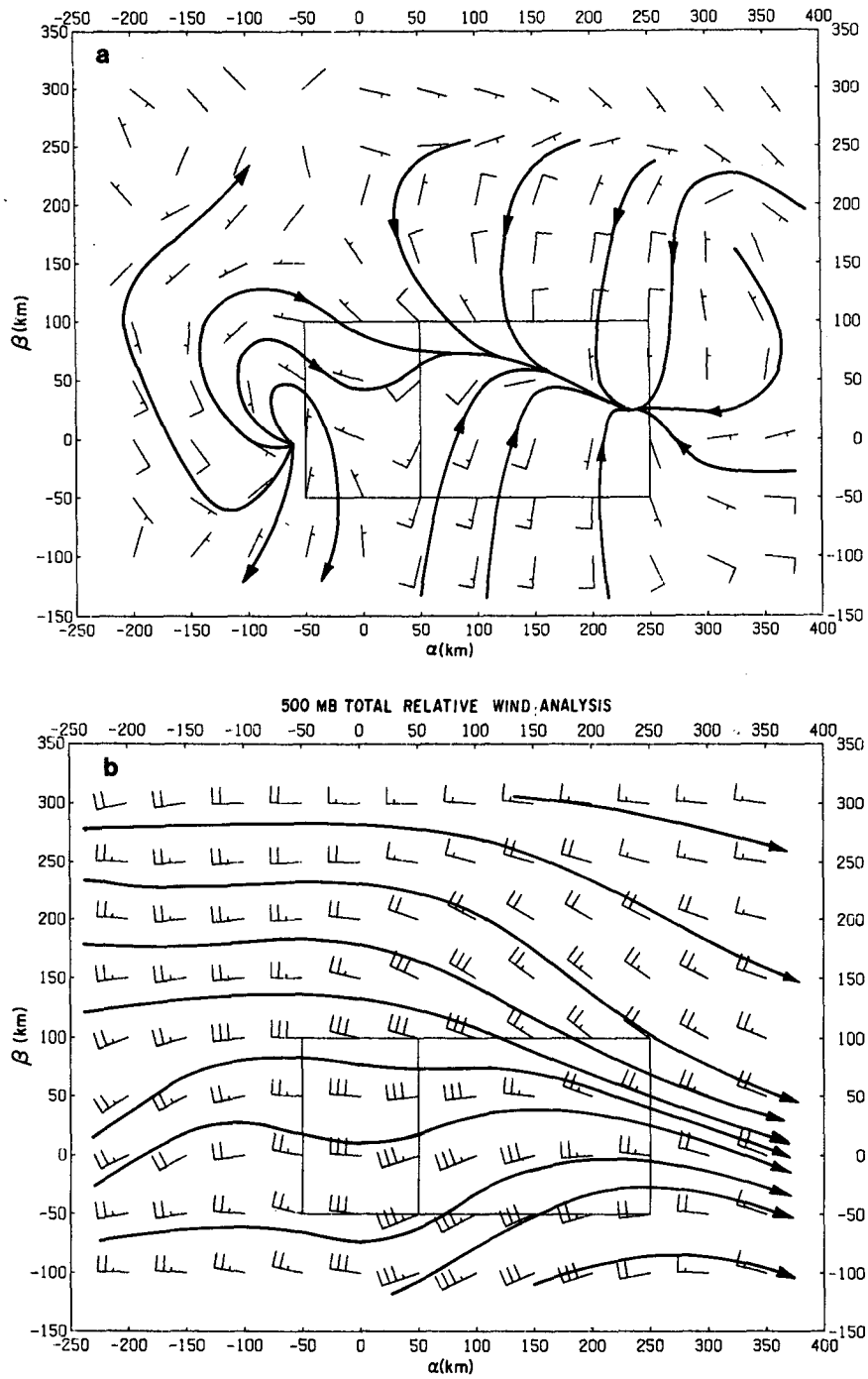


FIG. 5. (a) Mesoscale-bandpass 500 mb wind analysis. (b) Total relative winds at 500 mb. Full barb represents 5 m $s^{-1}$. (b) is produced by subtracting the velocity of the squall line (13.5 m $s^{-1}$ in the negative $\alpha$ direction) from the $T$ analysis (not shown here).

analysis (shown here in Fig. 5b since its subjective analysis counterpart was not shown in GH1). In this analysis, the mesoscale convergence is reflected in both confluence and speed convergence in the stratiform region.

At 200 mb (Fig. 6), the bandpass analysis shows regions of outflow (represented by outward pointing singularities in the steamline field) in both the convective and stratiform regions. The maxima in divergence (not shown) were located near $\alpha$ = 175 km, $\beta$ = 75 km and $\alpha$ = −125 km, $\beta$ = 125. The outflow in the stratiform region may have been associated with the top of the upper-tropospheric mesoscale updraft described in GH1, while the outflow in the

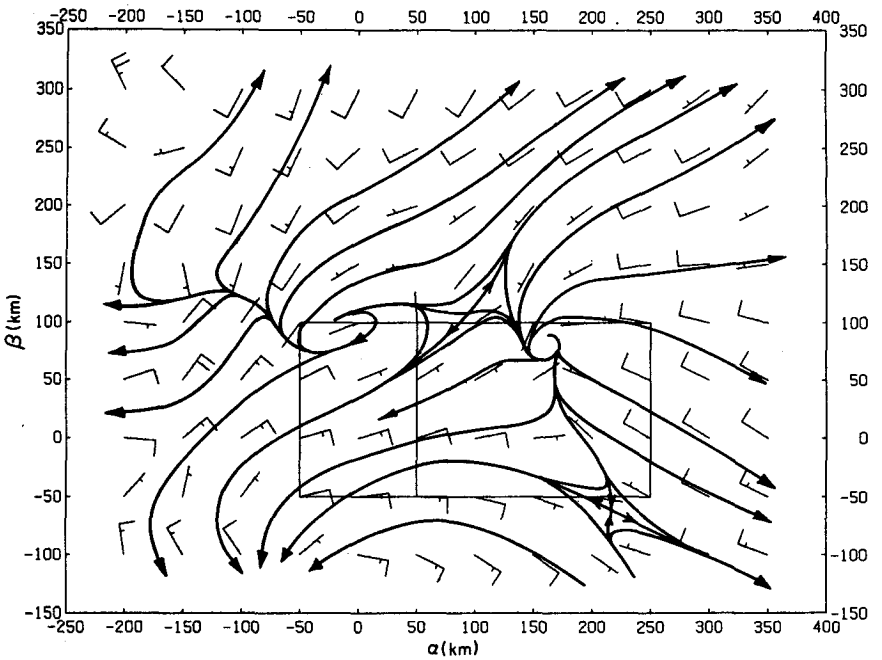


FIG. 6. Mesoscale-bandpass 200 mb wind analysis. Full barb represents 5 m $s^{-1}$.

convective region was more likely associated with the tops of deep convective cells along the squall line and in the preceding northeast–southwest line. Although the location of the centers of these outflow regions cannot be determined exactly from the data, we feel the general pattern of higher divergence at higher $\beta$ is consistent with the cell structure observed by radar. Figure 7 shows the composite field of the average maximum radar-echo top in the convective region. The highest echo tops (9–11.5 km) were located in the high-$\beta$ end of the convective region, coincident with and evidently producing the region of outflow seen in that region. In the low-$\beta$ half of the convective zone, the echo tops were below 8 km. These cells were too shallow to produce a strong effect at 200 mb, and, as will be shown in the thermodynamic analyses (Section 5), effects of their detrainment and spreading out were apparent at levels below 200 mb.

The divergence seen in the 200 mb bandpass analysis is consistent with the subjective analysis seen in Fig. 10 of GH1. That analysis also showed divergence over both the convective and stratiform regions, with stronger divergence in the higher-$\beta$ portion of the system.

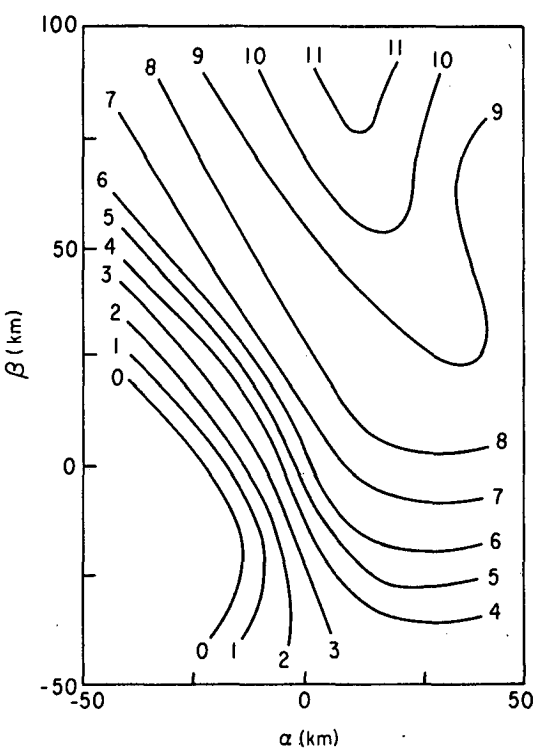


FIG. 7. Contours of average maximum echo top (km) in the convective region of the 12 September GATE squall system. Prior to contouring, average values were computed within horizontal grid squares 25 km in dimension from hourly data over the period 1300–1800 GMT. Based upon an average sampling distance from the radar of 60 km and a tilt-sequence interval of 2°, individual observations of echo tops are estimated to be accurate to ±1 km. However, the averaging reduces the uncertainty.

## 4. Divergence, vorticity and vertical velocity

The vertical profiles of divergence, vorticity and vertical velocity computed from the bandpass winds and averaged over the convective and stratiform regions are shown in Figs. 8 and 9. In general, the divergence and vertical velocity profiles are consistent with those derived from the subjective analysis in

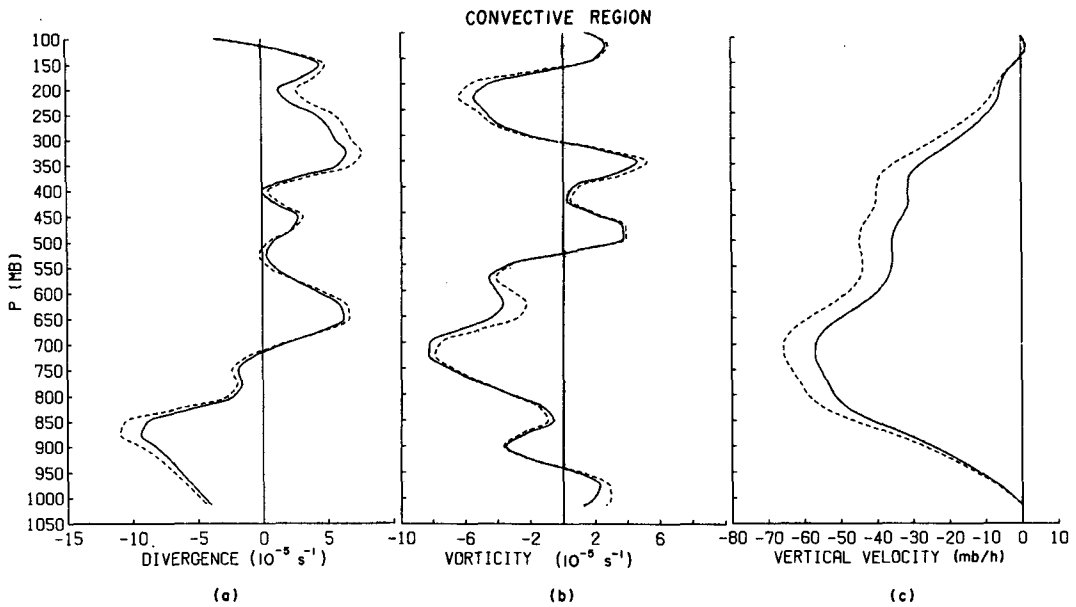


FIG. 8. Vertical profiles of (a) divergence, (b) relative vorticity and (c) vertical velocity for the convective region of the 12 September GATE squall system. Results are derived from objectively analyzed composite wind fields. Solid curves are for the mesoscale-bandpass filtered winds. Dashed curves are for the total winds.

GH1 and GH2 (See Fig. 12 of GH1). The following features are seen in both the subjective and objective analyses. In the convective region, convergence is located below about 700 mb, with divergence above, and mean upward motion at all levels (cf. Figs. 8a and c of this paper, Fig. 12 of GH1 and Fig. 5 of GH2).[1] In the stratiform region, convergence is seen in the midtroposphere, with divergence at low and high levels, and a mesoscale downdraft located below a mesoscale updraft (cf. Figs. 9a and c of this paper, Fig. 13 of GH1 and Fig. 5 of GH2).

Because 19, rather than 8, analysis levels are used in the objective analysis, more data are actually used, resulting in a real improvement in the vertical resolution. The profiles shown in Figs. 8 and 9 therefore show more detail in the vertical than do the subjective-analysis profiles in GH1 and GH2. One important result of the objective analysis is that the boundary between the mesoscale updraft and downdraft is found to be at about 520 mb rather than at the 650 mb level shown by the subjective analysis (compare Fig. 9c with Fig. 13 of GH1). This new result agrees better with the results of Johnson (1982) and Houze and Rappaport (1984), who found the level of zero vertical motion separating the mesoscale updraft and downdraft in the stratiform regions of other tropical mesoscale convective systems at 500 and 580 mb, respectively.[2]

The convective-region objective analysis shows a double maximum in divergence not seen in GH1. This difference is attributable to both an increase in the vertical resolution and to a decision in GH1 to ignore the speed given by a wind observation in the lower-$\alpha$, lower-$\beta$ corner of the convective region at 650 mb (see Fig. 7a of GH1). After more careful consideration of the radar echo tops seen in this portion of the convective region, it was decided that indeed there must be intense outflow associated with these shallow, though high-reflectivity echoes [greater than 40 dBZ in some locations].

In GH1 and GH2, we did not present calculations of vorticity. From Fig. 9, it can be seen that the peak vorticity in the stratiform region occurred at 650 mb, while the maximum convergence was at 500 mb. These peaks correspond to the vortex seen in the stratiform region at 650 mb in Fig. 4 and the convergent but less rotational wind pattern seen in the same region at 500 mb in Fig. 5. In a study of a midlatitude mesoscale convective system, which exhibited structure similar to that of a tropical squall line, Ogura and Liou (1980) found a similar offset in the peaks of convergence and vorticity in the stratiform region (Fig. 10). As in our case, the maximum

[1] In comparing the figures, note that the magnitude of the vertical velocity in the convective region is less in the objectively analyzed case because of the greater horizontal smoothing introduced by the objective analysis procedure. The shapes of the curves, however, should be comparable.

[2] The 0°C level in Houze and Rappaport's (1984) cases was at about 600 mb, while in Johnson's (1982) case it was between 550 and 600 mb.

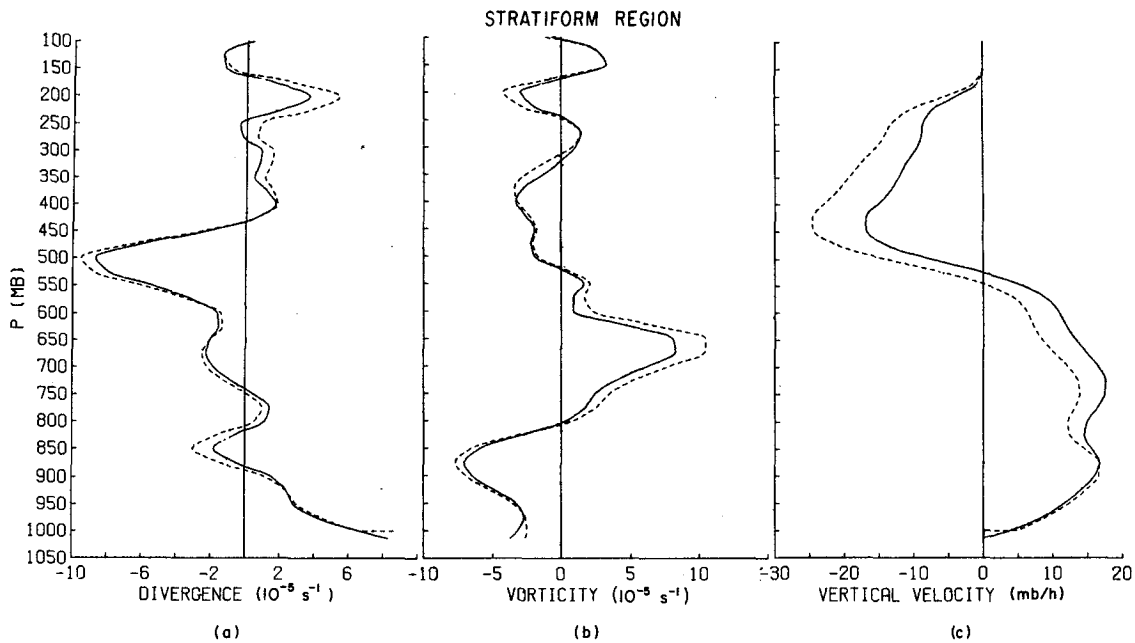


FIG. 9. Vertical profiles of (a) divergence, (b) vorticity and (c) vertical velocity for the stratiform region of the 12 September GATE squall system. Results are derived from objectively analyzed composite wind fields. Solid curves are for the mesoscale-bandpass filtered winds. Dashed curves are for the total winds.

of vorticity was about 100 mb below the level of maximum convergence.

## 5. Thermodynamic analysis

Vertical cross sections of mesoscale bandpass temperature (hereafter referred to as $T_B$) along $\beta$ = 100, 50, 0 and −50 km are shown in Figs. 11a–d. Similar cross sections are shown for bandpass specific humidity ($q_B$; Figs. 12a–d) and bandpass moist static energy[3] ($h_B$; Figs. 13a–d). Vertical cross sections of total moist static energy ($h_T$) are shown in Figs. 14a–d. Relative humidity is shown in Figs. 15a–d. The cross-section patterns are divided into pre-line, convective, stratiform and poststratiform regions. The following discussion will consider each of these regions in turn.

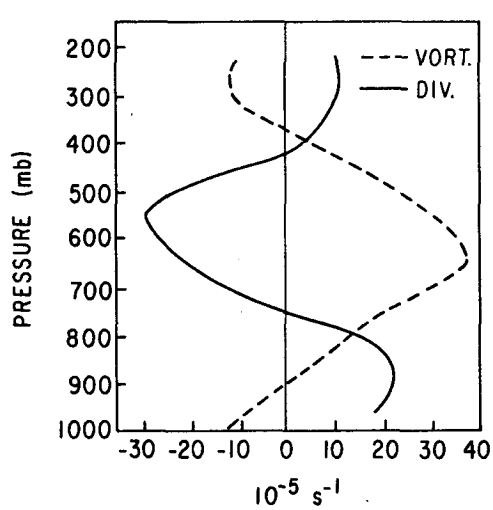


FIG. 10. Vertical profiles of divergence and vorticity in the stratiform region of a midlatitude mesoscale convective system. Curves apply at $x \approx -110$ km in Figs. 15 and 18 of Ogura and Liou (1980).

### a. *Pre-line region*

In the pre-line region, the $T_B$ and $q_B$ fields were quite weak and showed very little detail. Below the 600 mb level, however, both $T_B$ and $q_B$ increased in value with increasing $\beta$. Near the surface, both fields showed positive values at $\beta$ = 100 km (Figs. 11a and 12a) and negative values at $\beta$ = −50 km (Figs. 11d and 12d). These variations near the surface, together with the much weaker variation above the 600 mb level, indicate that the region ahead of the higher-$\beta$ portion of the squall line was more unstable. This is confirmed in Figs. 14a–d by the $h_T$ cross sections. The lesser instability ahead of the lower-$\beta$ end of the line was probably the result of stabilization by prior convection, which had been present in a northeast–southwest convective line immediately ahead of the squall line and in a squall line which passed through the GATE ship array the preceding evening.

[3] The moist static energy is defined as $c_pT + Lq + gz$, where $c_p$ is the specific heat at constant pressure, $L$ the latent heat of vaporation, $g$ the gravitational acceleration, $T$ temperature, $q$ specific humidity and $z$ is height.

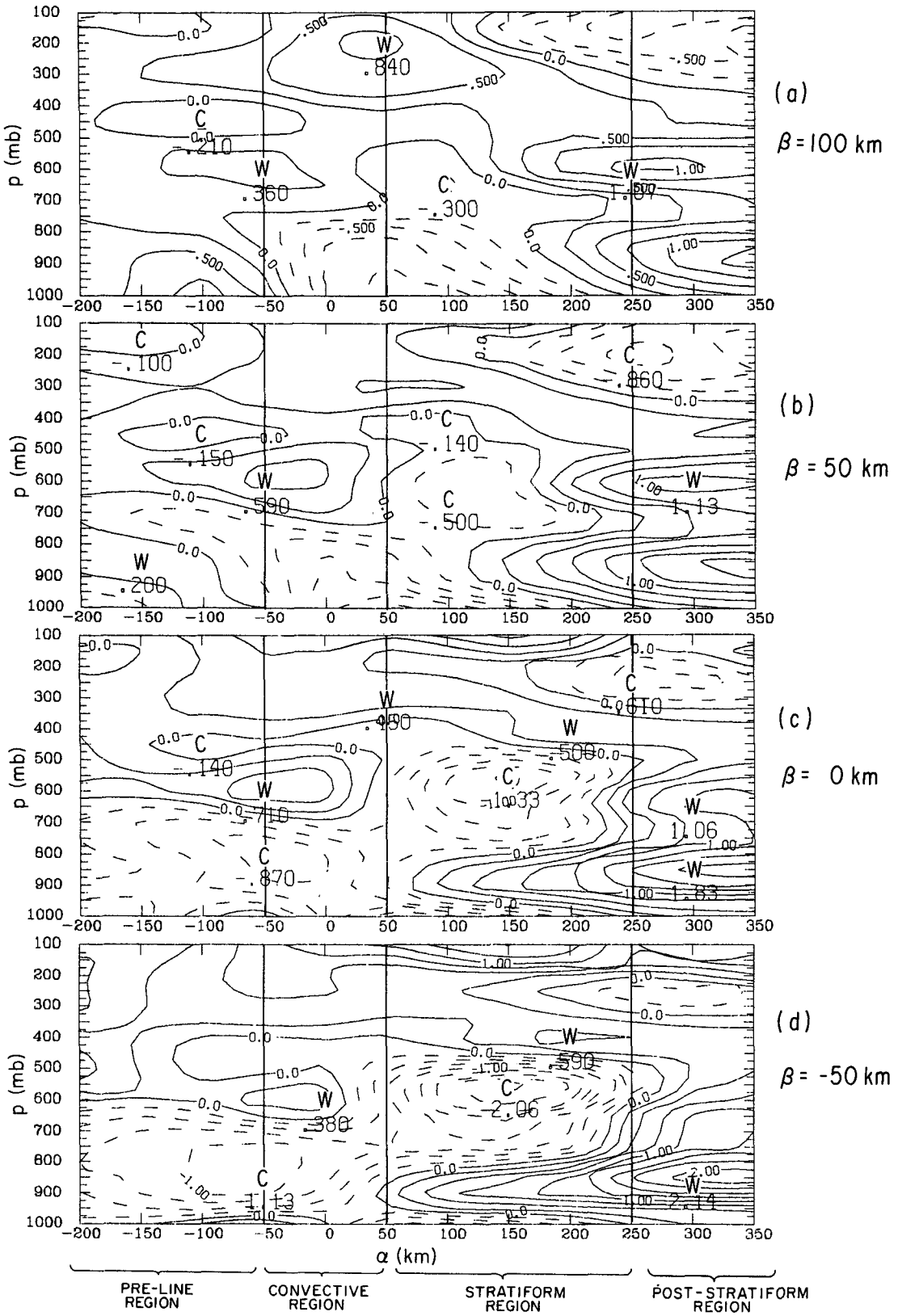


FIG. 11. Vertical cross sections of mesoscale-bandpass temperature (°C) along (a) $\beta$ = 100 km, (b) $\beta$ = 50 km, (c) $\beta$ = 0 and (d) $\beta$ = −50 km. Cross sections are perpendicular to the squall line and along the direction of system motion. Negative values are indicated by dashed contours. Large numerals indicate values at maxima (W) and minima (C) Each contour shows a 0.25°C change.

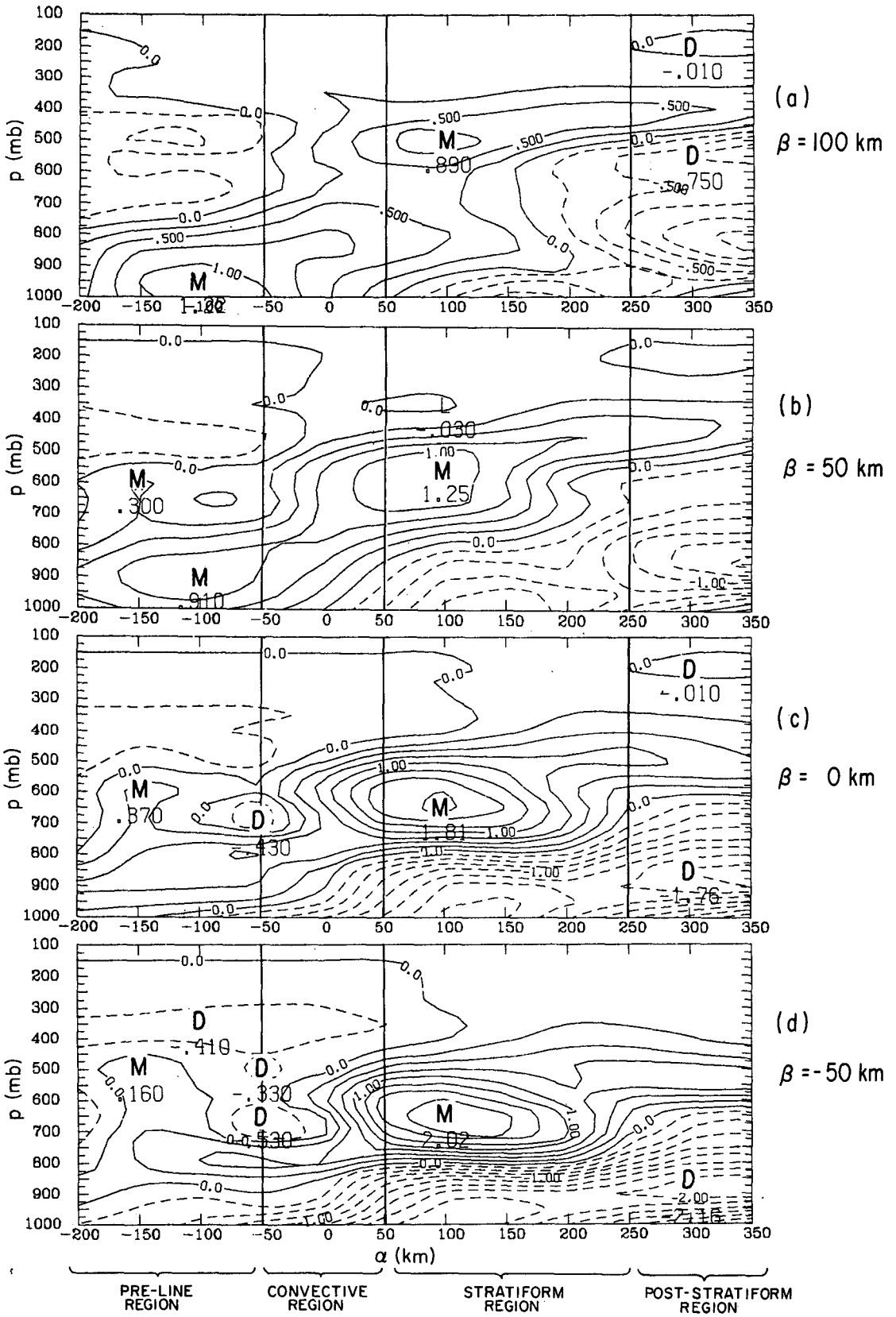


FIG. 12. Vertical cross sections of mesoscale-bandpass specific humidity (g kg$^{-1}$) along (a) $\beta$ = 100 km, (b) $\beta$ = 50 km, (c) $\beta$ = 0 and (d) $\beta$ = −50 km. Cross sections are perpendicular to the squall line and along the direction of system motion. Negative values are indicated by dashed contours. Contour interval is 0.25 g kg$^{-1}$.

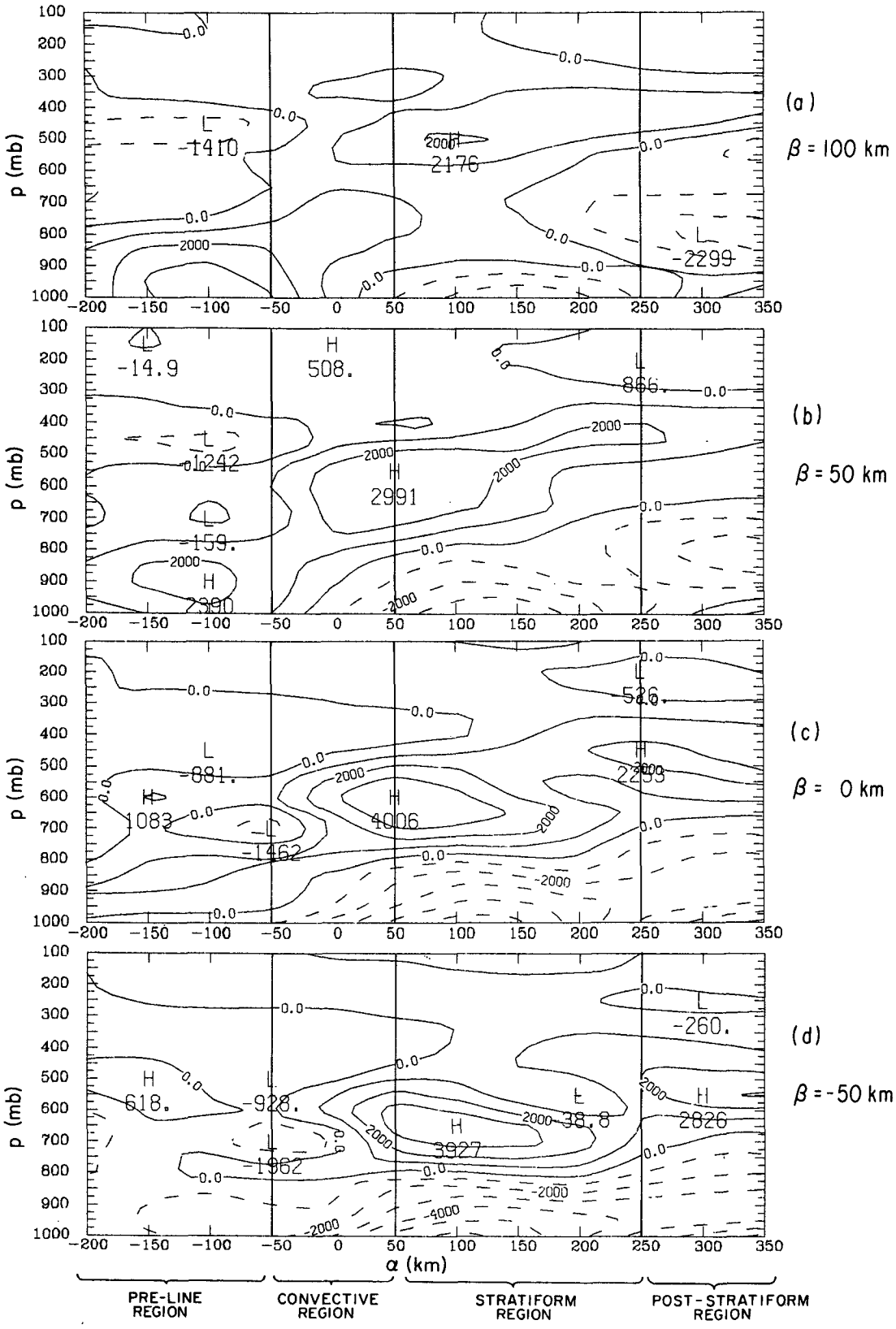


FIG. 13. As in Fig. 12 except for mesoscale-bandpass moist static energy (J kg$^{-1}$).

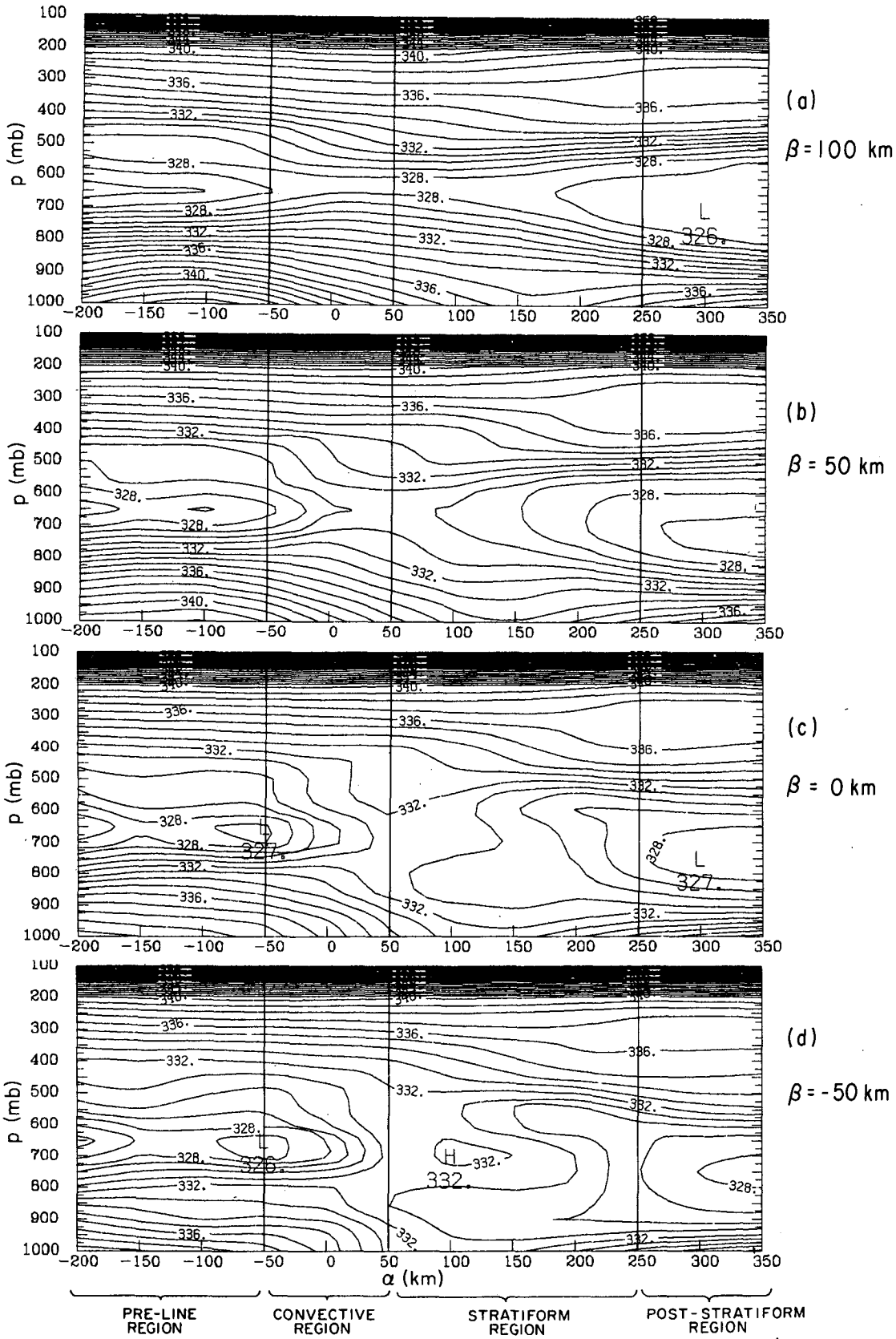


FIG. 14. As in Fig. 12 except for total moist static energy (kJ kg$^{-1}$).

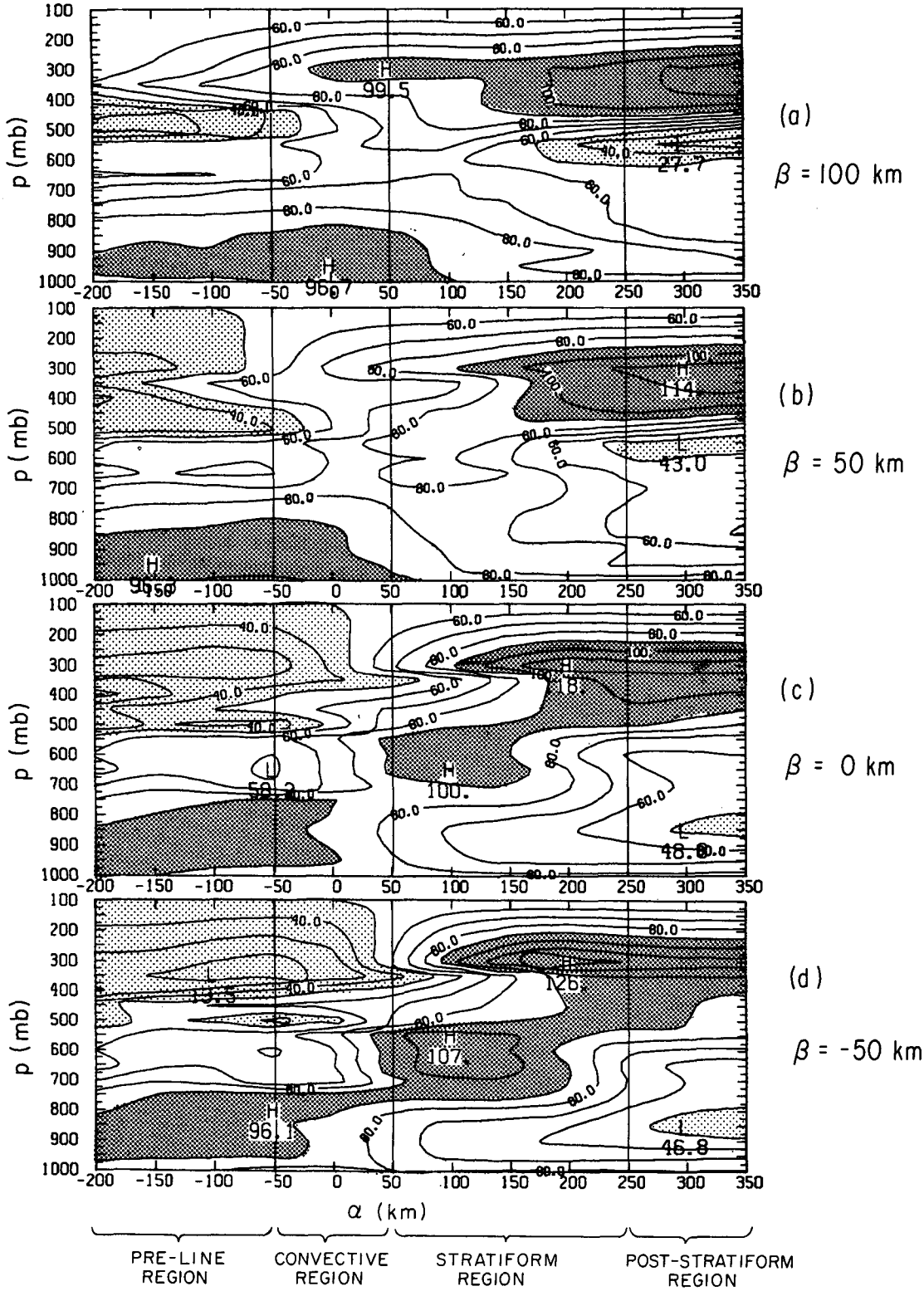


FIG. 15. Vertical cross sections of total relative humidity (percent) along (a) $\beta$ = 100 km, (b) $\beta$ = 50 km, (c) $\beta$ = 0 and (d) $\beta$ = −50 km. Cross sections are perpendicular to the squall line and along the direction of system motion. Values over 90 percent are shaded heavily. Values under 50 percent are shaded lightly. Large numerals indicate values at maxima (H) and minima (L). The relative humidity is computed over water at 650 mb and below and over ice at 450 mb and above, with linearly weighted averages of humidity over ice and water between 650 and 450 mb.

On 11 September, this preceding squall line moved through the area covered by the radar on board the ship *Researcher*. The progress of this earlier squall line is traced for times up to 2400 GMT 11 September by the isochrones in Fig. 16a. After 2400 GMT, the southern portion of this squall line continued to progress westward until it moved out of radar range. During the hours following 2400 on the 11th, convection began to develop into a quasi-stationary northeast–southwest line lying roughly along the northern edge of the region traversed by the earlier squall line. This northeast–southwest line persisted and intensified during the late morning of the 12th. The *Researcher* radar-echo pattern at 1000 GMT (Fig. 16a) is representative of this persistent line, and from its position relative to the isochrones of the preceding squall line its location along the northern edge of the wake of the earlier squall line is evident. The echo just northwest of *Researcher* at 1000 GMT, well before passage of the 12 September squall line, was one of the deepest and most intense echoes observed by its radar during Phase III of GATE. This observation confirms the presence of instability and surface convergence just to the north of the wake region of the 11 September squall line. In the afternoon, the 12 September squall line moved into the range of the *Researcher* radar. This squall line (located between the heavy arrows in Fig. 16b) moved southwestward along a path that intersected at a right angle the northeast–southwest line along the edge of the wake of the earlier squall line. While the 12 September squall line interacted with the northeast–southwest line, the northwestern half of the squall line encountered the more unstable environment ahead of that part of the line and directly encountered the northeast–southwest line. The deep cells in the high-$\beta$ portion of the convective region (Fig. 7) occurred during this interaction, while the shallow cells in the low-$\beta$ part of the convective region occurred where the southeastern half squall line moved through the region originally traversed by the previous squall. The less intense convection may be due in part to the continuing effects of the previous squall line's wake, to the effects of the outflow from the northeast–southwest convective line, and to the fact that the lower $\beta$ part of the squall line was not in direct contact with the northeast–southwest line. This configuration appears to have enhanced convergence in the higher-$\beta$ part of the squall line.

### b. *Convective region*

Although individual convective-scale features are not resolved by the objective analysis, the analyzed features located within the convective region are hypothesized to have resulted from the presence of convective updrafts and downdrafts along the squall line.

In the convective region the lowest values of $T_B$ occurred in the lower troposphere at all $\beta$ (Fig. 11). At $\beta = 0$ and $-50$, the lowest values of $q_B$ were also in the lower troposphere (Fig. 12c–d). Near the surface and at all $\beta$, both $T_B$ and $q_B$ also decreased from the front to the rear of the convective region, and low values extended into the stratiform region. The relative humidity, however, remained quite high. This suggests and is consistent with the presence of outflow of air from convective downdrafts, which according to Zipser (1977) and Houze (1977) were cool and nearly saturated in GATE.

Positive $T_B$ existed above the 650 mb level throughout the convective region. At all values of $\beta$ a local maximum existed at or near the 600 mb level, ranging in value from 0.4 to 0.7°K. This maximum appeared to extend into the pre-line region. The explanation for this feature is uncertain, but a possible one is subsidence which was compensating the convective updrafts. This is the level of maximum convective-region upward transport and in the absence of sufficient evaporation, warming would be expected at this level in response to subsidence. Compensating subsidence and lateral detrainment of warm air from still buoyant updrafts may also have produced the upper-tropospheric local maximum seen in $T_B$ near 300 mb in the higher-$\beta$ portion of the convective region.

At midlevels, a maximum of $q_B$ was located in the front of the stratiform region and extended into the convective region. The maximum occurred at 500 mb at $\beta = 100$ km (Fig. 12a) and at 650 mb at $\beta = -50$ km (Fig. 11d). This positive anomaly of moisture is one of the most significant features in this analysis and is probably due to the action of cumulus convection along the squall line. Cloud-top and/or lateral detrainment of water and ice from convective updrafts appear to be the most likely causes of this strong moistening. The feasibility of the cloud-top detrainment is consistent with the echo-top field shown in Fig. 7, which shows echo tops confined below 7 km when $\beta < 0$ km.

The bandpass moist static energy field (Fig. 13) in the middle troposphere follows the specific humidity field quite closely. The convection along the squall line appears therefore to be an important source of energy to the convective-region middle tropospheric air and provides the energy, primarily in latent form, for further upward motion and condensational heating in the mesoscale updraft.

### c. *Stratiform region*

In the stratiform region, the bandpass temperature and specific humidity patterns appear to consist of several layers, which are brought out best by the analysis at $\beta = 0$ km (Figs. 11c and 12c), but are

evident to some degree in each of the panels of Figs. 11 and 12.

Near the surface, the thin layer of cold air, which was noted in the preceding subsection and which we believe probably originated as outflow from convective downdrafts, extended across the rear boundary of the convective region into the stratiform region. Just above this cold surface layer, a layer of high-$T_B$ air lying between 800 and 950 mb extended from the poststratiform region into the stratiform region. This warm layer was evidently produced where the warming by adiabatic compression in the mesoscale downdraft (Fig. 9c) exceeded the cooling by evaporation of raindrops (Leary, 1980; see also Kamburova and Ludlam, 1966; Zipser, 1969, 1977; and Betts and Silva Dias, 1979). $T_B$ appears to have been greater at lower $\beta$ than at higher $\beta$ (compare Figs. 11a–d), probably because the rainfall was less at $\beta = 0$ and $-50$ km than at $\beta = 50$ km (Fig. 17), and the mesoscale downdraft was more intense at lower $\beta$ (please refer to Figs. 15a–c of GH2 and not to Figs. 15 and 16 of GH1, which as stated in GH2 were constructed without using all the available data). The $q_B$ field (Figs. 12a–d) is consistent with this reasoning. In the layer from 800 to 950 mb, the $q_B$ minimum is much lower in value at $\beta = -50$ km (Fig. 12d) than at $\beta = 100$ km (Fig. 11a), and the value increases monotonically with increasing $\beta$.

Just above the lower tropospheric maximum in $T_B$, a very deep layer of lower $T_B$ air was found in the stratiform region, extending from 800 to 450 mb. The lower portion of this layer of lower $T_B$ was colocated with the melting layer and was best defined by the analysis at $\beta = 50$ km and 0 km (Figs. 11b and c), but it was also evident at $\beta = 100$ and $-50$ km (Figs. 11a and d). Air sinking at these locations appears to have been cooled as melting and evaporation reduced the warming by adiabatic compression, which would have occurred in the mesoscale downdraft in the absence of precipitation. Leary and Houze (1979) showed the effectiveness of melting in producing a layer of cooling in the stratiform regions of GATE squall lines.

Above the melting level, from 650 to 450 mb, more cold air appears to have been present in the stratiform region. From Figs. 11a–d, it can be seen that this minimum of $T_B$ was analyzed to have been relatively weak at $\beta = 100$ kms but increasingly pronounced with decreasing $\beta$, being very strong at $\beta = -50$ km. Whether this cool layer is genuine or the result of erroneous sounding data is questionable. It is seen in the soundings launched from the NOAA Ship *Oceanographer* at 1513 GMT and from the Soviet Ship *Poryv* at 0833 on 12 September. That it may have been real is suggested by its appearance in both soundings, which were separated by 6 h and 300 km in actual time and space, though they were within 50 km of one another in $\alpha$–$\beta$ coordinates. However, both soundings exhibited suspiciously high lapse rates through portions of the 650–450 mb layer. A somewhat less intense cool layer is found in a sounding launched from the NOAA Ship *Researcher* at 1902 GMT. This additional sounding, together with the previously discussed consistency of the humidity and radar data, tends to increase the confidence in the soundings indicating presence of the cool spot.

The existence of this cool layer is not physically inconsistent with other observed features of the squall system. For example, the cool layer coincided in height with the layer of maximum convergence centered at the 500 mb level in the stratiform region (Fig. 9a). The converging flow at this level was entering the stratiform region both from the convective region (across $\alpha = 50$ km) and from the large-scale environment on both the low-$\beta$ and high-$\beta$ sides of the region (across $\beta = -50$ km and $\beta = 100$ km; see relative flow in Fig. 5b). The environmental air entering from the sides was probably largely unsaturated. Air entering from the convective region was probably a mixture of air detrained from cells and environmental air flowing around the cells. The air from cells would have been saturated and laden with condensate. Evaporation of the condensate detrained from cells into environmental air converging into the stratiform region could have produced or contributed to cooling in the 650–450 mb layer.

Other factors possibly explaining or contributing to the cooling in the 650–450 mb layer at low $\beta$ in the stratiform region may be suggested. The cooling may have been the result of negatively buoyant cloud-top air being detrained from the tops of the relatively shallow convective cells located in the lower-$\beta$ end of the convective region (Fig. 7). These cells were apparently initiated by strong low-level gust-front convergence acting on less unstable air left in the wake of the earlier squall line and/or northeast–southwest line (Section 5a, Fig. 16). This action would have led to parcels moving rapidly upward through cloud base but quickly encountering a low level of zero buoyancy through which they penetrated. Thus, shallow "overshooting" towers could have been produced in the midtroposphere and detrained anomalously cold air into the stratiform region.

Another mechanism that may have been involved in the production of the 650–450 mb cool layer is suggested by mesoscale modeling results. From Figs. 9c and 11, it is evident that the level of zero vertical motion in the stratiform region (at 520 mb in Fig. 9c) lay within the 650–450 mb cool layer, near the level where the cooling was greatest. It was pointed out by Rosenthal (1980) that if the base of a mesoscale updraft becomes unsaturated as a result of the convergence of dry air into its base, then dry stable ascent will occur and produce a cool layer at the base of the mesoscale updraft. Some evidence of very dry air entering the stratiform region in the layer from

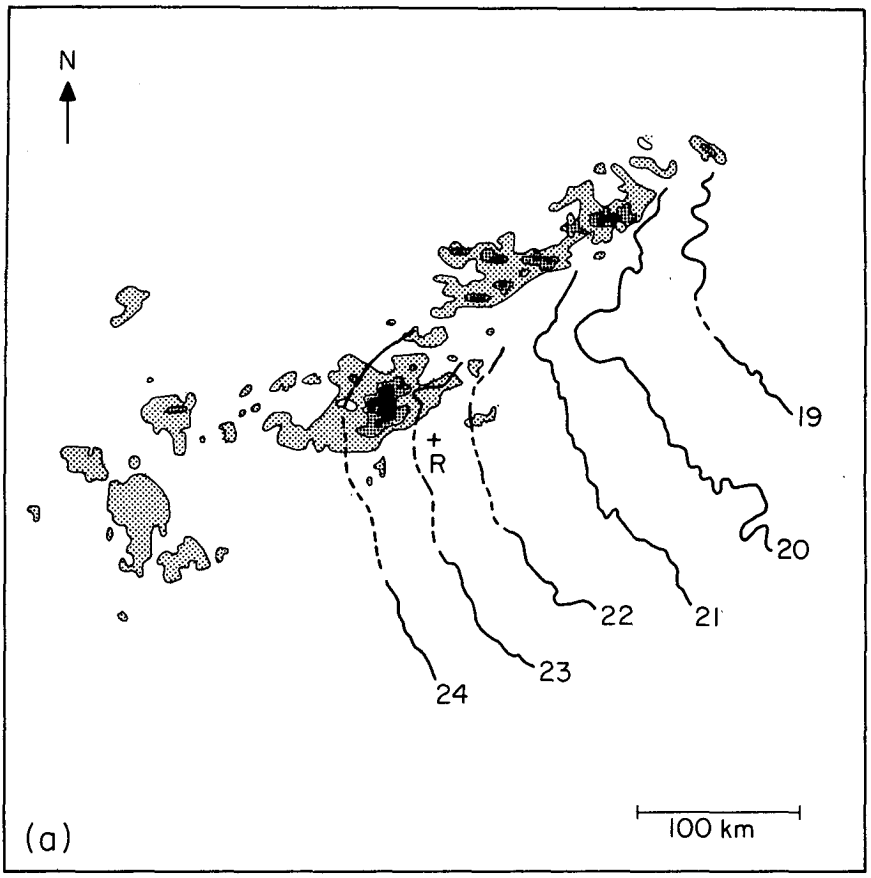
N
19
20
21
22
23
24
+
R
100 km
(a)

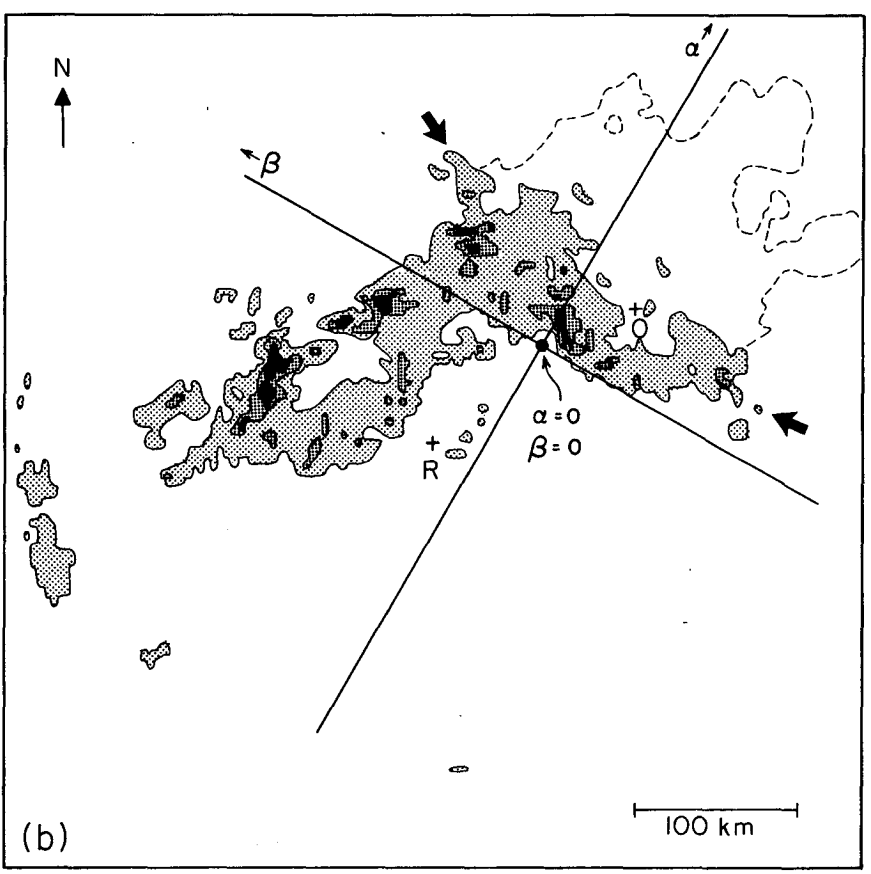
N
α
β
α = 0
β = 0
+
R
100 km
(b)

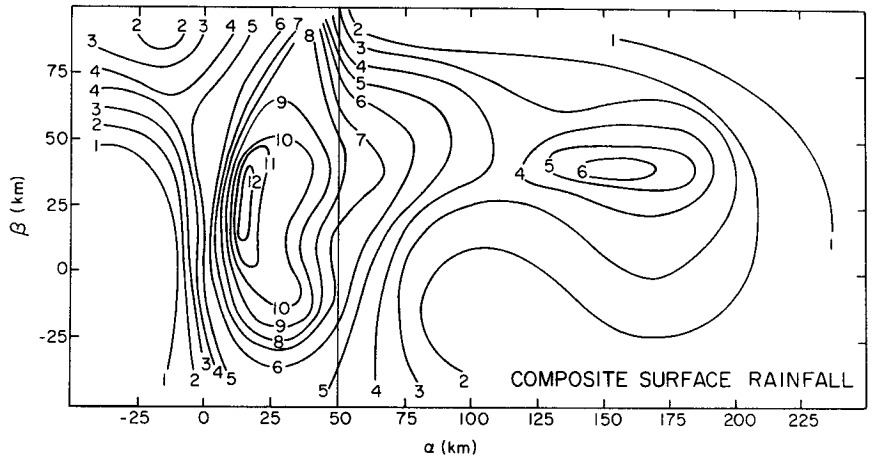


FIG. 17. Composite surface rainfall (mm $h^{-1}$) for the convective and stratiform regions of the 12 September GATE squall line. From Gamache and Houze (1983).

500 to 600 mb is suggested by the relative humidity analyses, particularly those in Figs. 15a and b. Air can be seen entering from the sides in the 500 mb relative wind analysis (Fig. 5b). Strong convergence is apparent from 450 to 550 mb in the stratiform region (Fig. 9). Perhaps more dry air enters than can be immediately moistened by evaporation.

Above the cool layers just described, an upper tropospheric layer of warm air, sloping downward toward the rear of the squall system, extended across the stratiform region. At $\beta$ = 100 km (Fig. 11a), this layer was located between 500 and 100 mb at $\alpha$ = 50 km and between 650 and 300 mb at $\alpha$ = 250 km. The layer was shallower but occupied the same general position at lower $\beta$ (Figs. 11b–d). This warm layer was associated with the mesoscale updraft, which was located in the upper troposphere of the stratiform region (Fig. 9c). The analysis in Fig. 15 indicates that saturation with respect to ice (water saturation was only found in the middle troposphere immediately behind the convection) through most of the mesoscale updraft. From Fig. 11, it appears that the positive temperature anomaly in the mesoscale updraft was generally between 0.2 and 0.5°C.

Prior to this study, no observational evidence regarding the temperature or moisture structure of the mesoscale updraft has been available. In calculations of heat transports, mesoscale updrafts have typically been estimated to have temperature perturbations of 1°C and to be water saturated (Leary and Houze, 1980; Houze and Cheng, 1981). The 0.2–0.5°C temperature anomaly seen here may, however, characterize a relatively weak example because of the strong relative flow (15–20 m $s^{-1}$) through the squall system at upper levels. In systems with less ventilation, heating from nearby convective updrafts might be more concentrated within the system. Rawinsonde observations of humidity at high levels, as always, are questionable. Nonetheless, the indication of this analysis that water saturation in the stratiform cloud was confined to a narrow zone at the rear of the active convective line, while further downwind (relative to the line) ice saturation prevailed, suggests that as convective-cell debris was advected toward the rear of the system it was at first water-saturated as a result of convective updraft motion but quickly became glaciated and ice-saturated as it moved further downwind. It has been pointed out that the heat released in the transition from water to ice saturation is surprisingly large, especially in a stratiform cloud (Orville and Hubbard, 1973; Orville *et al.*, 1984). This type of heating might have been involved in the development of the mesoscale updraft motion in the stratiform region downwind of the convective line.

FIG. 16. Radar observations of 11 and 12 September GATE squall-line systems. (a) Isochrones showing hourly position of the 11 September line from 1900–2400 GMT and reflectivity pattern at 1000 GMT on the 12th. The reflectivity pattern shows an intense southwest–northeast line of echoes that formed along the northern edge of the wake of the 11 September line. (b) Reflectivity pattern at 1400 GMT on the 12th showing the intersection of the southwest–northeast line bounding the wake of the 11 September squall line with the 12 September squall line (between the arrows), which was moving southwestward and was followed by a region of stratiform precipitation (enclosed by the dashed line). The reflectivity patterns and isochrones are from the radar on board the ship *Researcher* (labeled R). The stratiform area was delineated by the radar on the *Oceanographer* (labeled O). Shading thresholds in the reflectivity patterns are approximately 5, 39 and 43 dBZ.

At very high levels (above 300 mb), the rear of the stratiform region was characterized by a layer of negative $T_B$ (all panels of Fig. 11). This cool anomaly was located at and above the top of the stratiform cloud shield and extended into the poststratiform region. Johnson and Kriete (1982) found low temperature anomalies at the tops of stratiform cloud shields of winter monsoon cloud clusters and that these anomalies extended from the top of the troposphere into the lower stratosphere. Fritsch and Maddox (1981) have found similar cooling at and above the tops of the cloud shields of midlatitude convective complexes. Fritsch and Brown (1982) have suggested that this cool layer forms where the mesoscale updraft extends above the top of the cloud and dry adiabatic ascent of the stable air in the upper troposphere and lower stratosphere leads to the cold layer. Johnson and Kriete (1982) have noted that the cooling may also be explained by divergence of longwave radiative flux at the top of the stratiform cloud.

### *d. Poststratiform region*

In the poststratiform region, the most important features in the bandpass temperature pattern (Fig. 11) were the extension of the upper-level cool layer into this region from the stratiform region and the anomalously warm layer extending downward from the base of the cool layer ($\approx$300 mb) to the surface. This is an extension and a deepening of the warm layer seen in the stratiform region. The lower-tropospheric $T_B$ maximum and $q_B$ minimum are found in the poststratiform region. Apparently downward motion continues even after the cessation of precipitation (see Fig. 15 of GH2). In the absence of evaporational cooling, but yet in the presence of subsidence, the lower troposphere is warmer and drier than in the stratiform region. The bandpass specific humidity field (Fig. 12) is consistent with this view, as it shows lower $q_B$ in the poststratiform region where midtropospheric air is continually advected downward, even in the absence of evaporation of precipitation. Zipser (1977) noted that this warming tends to produce a mesolow to the rear of the stratiform precipitation, where the warmest lower tropospheric air exists and water loading is much less, immediately behind the squall line. The mesolow in the poststratiform region of the 12 September squall line has been further described and interpreted by Johnson and Nicholls (1983; see their Fig. 9).

## 6. Conclusions

Application of the objective analysis technique of Barnes (1964, 1973) and Maddox (1980) to the composite wind, temperature and humidity fields of the 12 September 1974 GATE squall line confirms and adds details to the subjective analyses carried out in GH1 and GH2. The divergence and vertical motion profiles in the convective and stratiform regions are generally similar to those found in GH1 and GH2. Again, the stratiform region is seen to have had a mesoscale downdraft in the lower troposphere and a mesoscale updraft aloft. However, the increased vertical resolution provided by the additional levels included in the objective analysis shows that the level of zero vertical motion bounding the mesoscale updraft and downdraft occurred at a somewhat higher level (520 mb) than was suggested by the previous studies (650 mb). This higher level agrees better with results obtained for other mesoscale convective systems by Ogura and Liou (1980), Johnson (1982) and Houze and Rappaport (1984).

Generally, the objective analysis of the thermodynamic fields revealed the basic structure expected for a tropical squall line. The thermodynamic structure of the convective region reflected the collective effects of cumulus-scale updrafts and downdrafts, while that of the stratiform and poststratiform regions was consistent with the presence of the mesoscale downdraft in the lower troposphere and the mesoscale updraft aloft. While the thermodynamic structure of the mesoscale downdraft has been fairly well documented in various earlier studies (Zipser, 1969, 1977; Houze, 1977; Ogura and Liou, 1980), the thermodynamic structure of the mesoscale updraft has been practically unknown heretofore. The mesoscale updraft in this case was found to be quite moist, saturated with respect to ice except just to the rear of the convective line, where the mesoscale updraft was water-saturated. Near the base of the mesoscale updraft, a layer of cool air was observed. Whether this cool layer, which was strongest in the southern part of the stratiform region, was genuine or the result of erroneous soundings could not be definitively determined; however, several plausible explanations have been offered for the cooling. Above this cool layer, the mesoscale updraft was, as expected, warmer than the large-scale environment, but with a maximum temperature anomaly of only 0.2–0.4°C. Near the top of the mesoscale updraft, in the rear half of the stratiform region, the temperature was lower than in the large-scale environment, probably as a result of either radiation or unsaturated mesoscale ascent.

The structure of the 12 September squall system was evidently modified substantially by interaction with the wake of an earlier squall line and with a northeast–southwest convective line that had formed on the northern boundary of the earlier wake. As the squall line moved southwestward through the GATE area, it intersected the nearly stationary southwest–northeast line. South of the intersection point, the 12 September squall line encountered air stabilized by outflow from the earlier squall line and/or the northeast–southwest line. At and north of the intersection, the squall line fed on very unstable large-scale environmental air. The configuration of this interaction

may also have enhanced convergence at and north of the intersection. Correspondingly, the convective towers in the northern half of the convective region of the squall line were very deep (echo tops 9–11.5 km) while in the southern half of the convective region cells were relatively shallow (echo tops generally below 8 km). To the rear of the convective line, advection of detrained condensate and water vapor from the tops of cells had a large impact on the temperature and humidity of the middle to upper troposphere of the stratiform region. Air of high humidity and peak moist static energy was observed at decidedly lower altitudes to the rear of the southern part of the convective line, where the cells were shallower, and at higher levels behind the northern part of the line.

The composite analyses of the 12 September squall system presented in this paper and its predecessors GH1 and GH2 have increased our knowledge of the convective and stratiform components of a mesoscale convective cloud system. Composite analysis, however, is limited to resolving the grosser structure that persists over a considerable portion of a system's lifetime. To understand more fully the relationship between the convective and stratiform regions and the lifecycle of the mesoscale system, attention should be focussed on the squall circulation at specific times rather than over long composite time periods. This focus may be achieved by performing detailed mesosynoptic analysis over relatively short time periods when standard data are highly supplemented by aircraft data, or through the use of Doppler radar observations (e.g., Sommeria and Testud, 1984).

*Acknowledgments.* This research was supported by the National Science Foundation under Grants ATM80-17327 and ATM82-14866.

## REFERENCES

Barnes, S. L., 1964: A technique for maximizing details in numerical weather map analysis. *J. Appl. Meteor.*, **3**, 396–409.

——, 1973: Mesoscale objective map analysis using weighted time series observations. NOAA Tech. Memo. ERL NSSL-62, 60 pp. [NTIS CON-73-10781.]

Betts, A. K., 1978: Convection in the tropics. *Meteorology over the Tropical Oceans,* Roy. Meteor. Soc., 105–132.

——, and M. F. Silva Dias, 1979: Unsaturated downdraft thermodynamics in cumulonimbus. *J. Atmos. Sci.*, **36**, 1061–1071.

Chen, Y.-H., and E. J. Zipser, 1982: The role of horizontal advection of hydrometeors in the water budget of a large squall line system. *Preprints 12th Conf. on Severe Local Storms,* San Antonio, Amer. Meteor. Soc., 335–358.

Fitzjarrald, D. R., and M. Garstang, 1981a: Vertical structure of the tropical boundary layer. *Mon. Wea. Rev.*, **109**, 1512–1526.

——, and ——, 1981b: Boundary-layer growth over the tropical ocean. *Mon. Wea. Rev.*, **109**, 1762–1772.

Fritsch, J. M., and R. A. Maddox, 1981: Convectively driven mesoscale weather systems aloft. Part I: Observations. *J. Appl. Meteor.*, **20**, 9–19.

——, and J. M. Brown, 1982: On the generation of convectively driven mesohighs aloft. *Mon. Wea. Rev.*, **110**, 1554–1563.

Gamache, J. F., 1983: A composite analysis of a tropical squall-line system. Ph.D. dissertation, University of Washington, 318 pp.

——, and R. A. Houze, Jr., 1982: Mesoscale air motions associated with a tropical squall line. *Mon. Wea. Rev.*, **110**, 118–135.

——, and ——, 1983: Water budget of a mesoscale convective system in the tropics. *J. Atmos. Sci.*, **40**, 1835–1850.

Houze, R. A., Jr., 1977: Structure and dynamics of a tropical squall-line system. *Mon. Wea. Rev.*, **105**, 1540–1567.

——, and A. K. Betts, 1981: Convection in GATE. *Rev. Geophys. Space Phys.*, **19**, 541–576.

——, and C.-P. Cheng, 1981: Inclusion of mesoscale updrafts and downdrafts in computations of vertical fluxes by ensembles of tropical clouds. *J. Atmos. Sci.*, **38**, 1751–1770.

——, and P. V. Hobbs, 1982: Organization and structure of precipitating cloud systems. *Advances in Geophysics,* **24**, Academic Press, 225–315.

——, and E. N. Rappaport, 1984: Air motions and precipitation structure of an early summer squall line over the eastern tropical Atlantic. *J. Atmos. Sci.*, **41**, 553–574.

Johnson, R. H., 1982: Vertical motion in near-equatorial winter monsoon convection. *J. Meteor. Soc. Japan,* **60**, 682–690.

——, and D. C. Kriete, 1982: Thermodynamic and circulation characteristics of winter monsoon tropical mesoscale convection. *Mon. Wea. Rev.*, **110**, 1898–1911.

——, and M. E. Nicholls, 1983: A composite analysis of the boundary layer accompanying a tropical squall line. *Mon. Wea. Rev.*, **111**, 308–319.

Kamburova, P. L., and F. H. Ludlam, 1966: Rainfall evaporation in thunderstorm downdrafts. *Quart. J. Roy. Meteor. Soc.*, **92**, 510–518.

Leary, C. A., 1980: Temperature and humidity profiles in mesoscale unsaturated downdrafts. *J. Atmos. Sci.*, **37**, 1005–1012.

——, and R. A. Houze, Jr., 1979: Melting and evaporation of hydrometeors in precipitation from the anvil clouds of deep tropical convection. *J. Atmos. Sci.*, **36**, 669–679.

——, and ——, 1980: The contribution of mesoscale motions to the mass and heat fluxes of an intense tropical convection system. *J. Atmos. Sci.*, **37**, 784–796.

Maddox, R. A., 1980: An objective technique for separating macroscale and mesoscale features in meterological data. *Mon. Wea. Rev.*, **108**, 1108–1121.

——, and T. H. Vonder Haar, 1979: Covariance analyses of satellite derived mesoscale wind fields. *J. Appl. Meteor.*, **18**, 1327–1334.

Ogura, Y., and M. T. Liou, 1980: The structure of a midlatitude squall line: A case study. *J. Atmos. Sci.*, **37**, 553–567.

Orville, H. D., and K. Hubbard, 1973: On the freezing of liquid water in a cloud. *J. Appl. Meteor.*, **12**, 671–676.

——, Richard D. Farley and J. H. Hirsch, 1984: Some surprising results from simulated seeding of stratiform-type cloud. *J. Climate Appl. Meteor.*, **23**, 1585–1600.

Rosenthal, S. L., 1980: Numerical simulation of tropical cyclone development with latent heat release by the resolvable scales, II. Propagating small-scale features observed in the pre-hurricane phase. Tech. Rep. ERL413-AOML29, NOAA Environ. Res. Lab., Boulder, CO, 43 pp. [NTIS PE81-176588.]

Sommeria, G., and J. Testud, 1984: COPT 81: A field experiment designed for the study of dynamics and electrical activity of deep convection in continental tropical regions. *Bull. Amer. Meteor. Soc.*, **65**, 4–10.

Zipser, E. J., 1969: The role of organized unsaturated convective downdrafts in the structure and rapid decay of an equatorial disturbance. *J. Appl. Meteor.*, **8**, 799–814.

——, 1977: Mesoscale and convective-scale downdrafts as distinct components of squall-line circulation. *Mon. Wea. Rev.*, 1568–1589.